Clim Dyn
DOI 10.1007/s00382-017-3625-x

Remote impact of North Atlantic sea surface temperature on rainfall in southwestern China during boreal spring

Gang Li[1] · Jiepeng Chen[2] · Xin Wang[2] · Xia Luo[3] · Daoyong Yang[1] · Wen Zhou[4] · Yanke Tan[3] · Hongming Yan[5]

Received: 13 October 2015 / Accepted: 8 March 2017

Abstract As an important oceanic signal, the North Atlantic sea surface temperature (SST) affects not only the climate variability over East China and Northeast China but also can affect climate variability over southwestern China (SWC). Based on station rainfall data and reanalysis datasets, the present study investigates the relationship of North Atlantic SST with SWC rainfall during boreal spring for the period 1979–2016. The results show that there is a significant positive correlation between North Atlantic SST and SWC rainfall during boreal spring. The atmospheric circulation over southern Asia associated with North Atlantic SST is favorable for positive rainfall anomalies. Further analyses show that North Atlantic SST can induce a North Atlantic–western Russia–western Tibetan Plateau–SWC (NRTC) teleconnection wave train from upper level to low level. At low level, two anomalous anticyclones are found over the mid-high latitude of North Atlantic and the western Tibetan Plateau, and two anomalous cyclones are observed over the western Russia and Bay of Bengal (BOB), respectively. The NRTC teleconnection wave train plays a bridging role between the North Atlantic SST and SWC rainfall during boreal spring. Both the observational analysis and two numerical experiments suggest that the North Atlantic SST during boreal spring can induce an anomalous cyclone over BOB by the NRTC teleconnection pattern. The anomalous cyclone over BOB favors moisture transport to SWC, accompanying with significant anomalous ascending motion, and thus results in positive rainfall anomalies in SWC during boreal spring.

1 Introduction

It is well known that southwestern China (SWC) is a region of low-latitude highlands (Tao et al. 2013), which is characterized by very complex geographic features (Fig. 1a). Administratively, SWC includes Sichuan, Yunnan, and Guizhou Provinces and Chongqing Shi, which are indicated by red, yellow, green, and cyan shading in Fig. 1b, respectively (Yan et al. 2013).

SWC rainfall is uniquely influenced by the complex topography and the monsoon circulation (Ma et al. 2006; Li et al. 2013; Wang et al. 2012, 2013a). Besides, SWC rainfall is mainly characterized as a wet season and a dry season (Zhang et al. 2014). As suggested by Zhang et al. (2014), the wet season is mainly from May to September, and the dry season is mainly from October to the following April. In general, positive rainfall is observed in SWC during the wet season, while less rainfall tends to appear during the dry season (Qin et al. 1997; Cheng et al. 2009). Besides, it should be mentioned that the transition period between wet and dry seasons is very short. Therefore, SWC is vulnerable to floods and droughts, which can result in enormously societal and economic losses. Indeed, several severe droughts have hit SWC since 2000 (Liu et al. 2007; Mao et al. 2007), including a severe drought from boreal

✉ Xin Wang
wangxin@scsio.ac.cn

[1] Xichang Satellite Launch Center, Xichang, China

[2] State Key Laboratory of Tropical Oceanography, South China Sea Institute of Oceanology, Chinese Academy of Sciences, Guangzhou, China

[3] College of Meteorology and Oceanography, PLA University of Science and Technology, Nanjing, China

[4] Guy Carpenter Asia-Pacific Climate Impact Centre, School of Energy and Environment, City University of Hong Kong, Hong Kong, China

[5] Yunnan Climate Center, Kunming, China

Published online: 21 March 2017

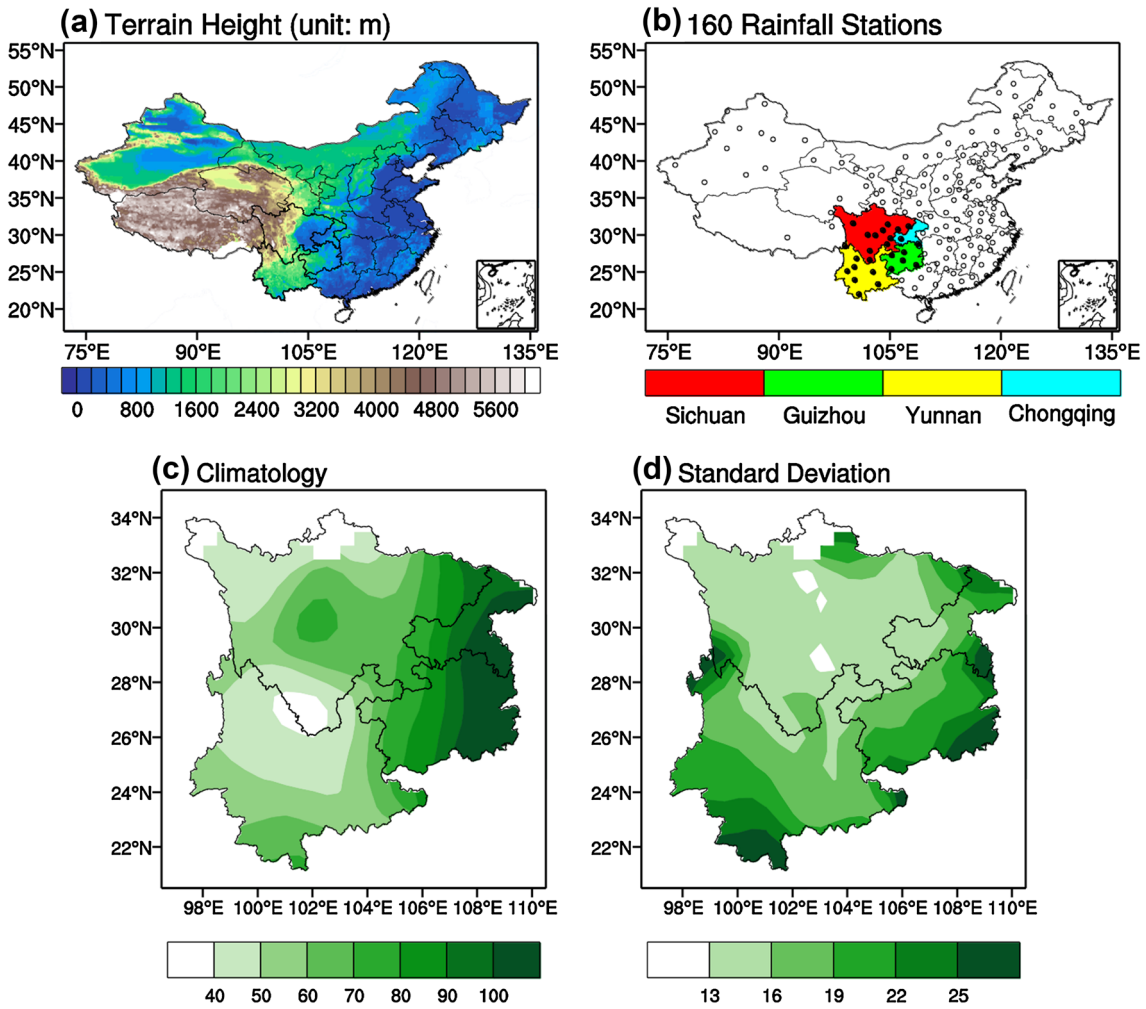

Fig. 1 **a** Terrain height (*shading*, m) of China and location (*black curves*) of SWC. **b** The distribution of 160 rainfall stations. The *black filled dots* are the 26 stations in SWC, which are used to define the SWC rainfall index (SWI). The areas shaded by *red, green, yellow*, and *cyan* indicate Sichuan, Guizhou, Yunnan, and Chongqing shi, respectively. **c** Climatology (mm month^{-1}) and **d** standard deviation (mm month^{-1}) of MAM (March–April–May) rainfall in SWC

autumn 2009 to boreal spring 2010, which was the driest event with the lowest percentage of rainfall anomalies and the most non-rain days in the past 50 years (Yang et al. 2012). This drought event left several million people short of drinking water, and the economic losses reached nearly 30 billion dollars according to a survey by the Ministry of Civil Affairs (Yang et al. 2012). In addition, in June 2011, a severe rainstorm hit Sichuan, Guizhou, and Yunnan Provinces, affecting more than 4 million people and causing enormous economic losses (nearly 1.6 billion dollars). Furthermore, in recent years, the coupling of extreme climate events (e.g., drought followed immediately by flooding), which may trigger natural hazards such as landslides, has occurred more frequently in SWC (Yang et al. 2012).

Considering the impact of severe floods and droughts on the societal and economic development in SWC, it is necessary to investigate the possible mechanisms that govern rainfall variability in this region. In fact, SWC rainfall variability has become an important area of research in recent years. Previous studies have revealed that SWC rainfall is characterized by significant spatiotemporal variability (Li et al. 2010; Jiang and Li 2011; Zhang et al. 2014). They demonstrated that the first mode of rainfall variability in SWC during both the wet and dry season is characterized by a homogeneous pattern. These homogeneous patterns show significant interannual and interdecadal variability (Jiang and Li 2011; Wang et al. 2013b, 2013c; Zhang et al. 2014; Jiang et al. 2015). Zhang et al. (2014) showed that the first mode has a quasi-biennial oscillation on interannual time scales. Jiang and Li (2011) revealed that less rainfall appeared in SWC before the 1980s, while positive rainfall was observed after the 1990s. In addition, the second mode of rainfall variability during both the wet and dry seasons

in southwestern China is characterized by a dipole-like structure (Zhang et al. 2014).

The relationship between SWC rainfall and large-scale climatic systems has been investigated in many studies. For instances, previous studies have demonstrated that sea surface temperature (SST) in both the Pacific and Indian Oceans can influence SWC rainfall through atmospheric circulation (Yan et al. 2005; Wang et al. 2009; Huang et al. 2012; Jiang et al. 2013; Cao et al. 2014). The snow cover over Tibetan Plateau is an important factor that affects rainfall variability in SWC due to its thermodynamic effects (Zou and Gao 2007; Li et al. 2011). The Arctic oscillation can also exert a pronounced impact on SWC rainfall variability through atmospheric anomalies over tropical regions (Jiang and Li 2011; Yang et al. 2012; Huang et al. 2012). In addition, an important factor that influences SWC rainfall variability is the North Atlantic Oscillation (NAO) (Xu et al. 2012; Song et al. 2014; Feng et al. 2014). In fact, many studies have demonstrated that NAO has a close relationship with East Asian Monsoon (Wu et al. 2009, 2012; Zheng et al. 2016). Wu et al. (2012) revealed that both observational and numerical results show that spring NAO can exert significant influence on the relationship between the East Asian summer monsoon (EASM) and ENSO. Zheng et al. (2016) further pointed out that the relationship between spring NAO and EASM is modulated by the summer NAO. Besides, the NAO may trigger a large-scale wave train pattern, which can induce an anomalous anticyclone over subtropical Asia, and then affect SWC rainfall (Xu et al. 2012).

Some studies have suggested that North Atlantic SST shows pronounced interdecadal to multidecadal variability, which can influence both global and local climate variability (Kushnir 1994; Enfield et al. 2001; Yu et al. 2015). In particular, many studies have pointed out that North Atlantic SST can influence the climate variability over East Asia through a North Atlantic–Asia teleconnection (Gu et al. 2009; Wang et al. 2011; Wu et al. 2011, 2012; Kim et al. 2013, 2014; Wu and Zhang 2015). For example, Gu et al. (2009) suggested that North Atlantic SST during boreal winter can influence the following East Asian summer monsoon (EASM) on decadal time scales. On interannual time scales, Wang et al. (2011) revealed that North Atlantic SST during boreal summer can influence the subsequent East Asian winter monsoon, which may favor initiating an El Niño event during boreal winter. In addition, North Atlantic SST during boreal spring can exert impact on the EASM and summer temperatures in northeast China through a Rossby wave train extending from Europe to Asia on interannual time scales (Wu et al. 2011). Wu et al. (2012) suggested that the North Atlantic SST can excite downstream teleconnections of a distinct Rossby wave train prevailing over the northern Eurasia, and then influence EASM. Besides, the relationship between NAO and ENSO is influenced by North Atlantic SST (Wu and Zhang 2015). However, the relationship between North Atlantic SST and SWC rainfall is unclear. On the other hand, compared to the studies on SWC rainfall in other seasons, much less attention has been paid to SWC rainfall variability during the boreal spring. Moreover, it should be mentioned that rainfall in boreal spring is important for agricultural activities in SWC. Therefore, some important issues need to be addressed in this study. First, we will reveal the relationship between North Atlantic SST and SWC rainfall during boreal spring. Second, the possible mechanisms will be investigated.

In Sect. 2 below, we describe the datasets and analysis methods used in this study. In Sect. 3, we investigate the relationship between North Atlantic SST and rainfall over southwestern China during boreal spring. In Sect. 4, possible physical mechanisms responsible for this relationship are investigated. In Sect. 5, we conduct the numerical experiments to demonstrate the results in Sect. 4. Section 6 provides a summary and discussion.

2 Datasets, methods and model

Several datasets are used in this study. The atmospheric circulation data is from the National Centers for Environmental Prediction–National Center for Atmospheric Research (NCEP–NCAR) reanalysis on a 2.5° × 2.5° grid, which is available from 1948 forward (Kalnay et al. 1996). The SST used in this study is obtained from the monthly mean Hadley Centre Sea Ice and Sea Surface Temperature dataset (HadISST) (Rayner et al. 2003). It has a horizontal resolution of 1° × 1° from 1870 forward. In addition, the accumulated monthly rainfall data at 160 stations in China (the locations of these 160 stations are shown in Fig. 1b) is used. This dataset is obtained from the Chinese Meteorological Data Center (http://cmdp.ncc.cma.gov.cn). The station rainfall data is available from 1951 forward.

Our analyses cover the period from 1979 to 2016. The boreal spring in this article is defined as March–April–May (MAM). For all of these datasets, anomalies are computed as departures from the 1979–2016 climatology, and a linear trend is removed before the analyses. Regression analyses are used in this study. The Student's t test is employed to examine the confidence level of the regression analyses. Besides, canonical correlation analysis (CCA) is used to identify major covariation modes between MAM rainfall in SWC and the simultaneous North Atlantic SST (Bretherton et al. 1992).

We calculate the vertically integrated moisture flux (from surface to 300 hPa) in this study. The vertically integrated moisture flux is calculated according to the Eq. (1):

$$Q = -\frac{1}{g}\int_{psfc}^{300\ \mathrm{hPa}} \left(q\vec{V}\right)\mathrm{d}p \tag{1}$$

where g is gravity, q is specific humidity, $\vec{V}$ is wind field, $psfc$ is surface pressure, and p is pressure.

To investigate the variability of wave activity, the wave activity F_s is given as in Plumb (1985):

$$F_s = p\cos\varphi \times \begin{pmatrix} v'^2 - \frac{1}{2\Omega a \sin 2\varphi}\frac{\partial(v'\Phi')}{\partial\lambda} \\ -u'v' + \frac{1}{2\Omega a \sin 2\varphi}\frac{\partial(u'\Phi')}{\partial\lambda} \\ \frac{2\Omega\sin\varphi}{S}\left[v'T' - \frac{1}{2\Omega a \sin 2\varphi}\frac{\partial(T'\Phi')}{\partial\lambda}\right] \end{pmatrix} \tag{2}$$

where $S = \frac{\partial\hat{T}}{\partial z} + \frac{\kappa\hat{T}}{H}$ is the static stability; the caret indicates an area-average over the area north of 20°N; p is the pressure; a is the radius of the earth; φ and λ are latitude and longitude, respectively; Φ is geopotential height, and Ω is the earth's rotation rate. The prime denotes deviation from the zonal mean.

To further demonstrate the observed influence of MAM North Atlantic SST on the simultaneous SWC rainfall, the NCAR Community Atmospheric Model version 5 (CAM5) is used to examine the response of atmospheric circulation to the North Atlantic SST. A complete description of this model version is available online at http://www.cesm.ucar.edu/models/cesm1.0/cam/docs/description/cam5_desc.pdf. CAM5 model is able to reproduce the climate features as observed (Liu et al. 2015). Therefore, two kinds of numerical experiments are provided in this study by the CAM5 model.

For the first experiment, CAM5 is forced by the climatological SST, referred to as CLIM_EXP. The control experiment (CTL) is driven by climatological SST, and is used to derive the climatological state. To investigate the impacts of the boreal spring North Atlantic SST on the simultaneous atmospheric circulation, we design two sensitivity experiments. Before conducting these two experiments, we first calculate the composite difference of MAM North Atlantic SST anomalies between the positive and negative MAM NAI years (figure not shown), which is selected based on the criterion of ±0.5 standard deviation of MAM NAI (Table 1). It is noted that significantly positive SST anomalies appears in the middle-high latitudes of North Atlantic, bearing strong resemblance to the results shown in Fig. 3b. Based on this result, the composite difference of SST anomalies in the mid-high latitudes of North Atlantic (45°–65°N, 30°W–10°E) is imposed onto the boreal spring North Atlantic SST climatology, which is referred to as the positive sensitivity experiment. Next, the composite difference of SST anomalies is inversed by multiplying −1, and then the inversed SST pattern is imposed onto the MAM North Atlantic SST climatology, forming a negative sensitivity experiment. All experiments are integrated for 30 years, and the last 20 years are used to construct a 20-member ensemble mean to reduce the model uncertainties resulting from initial conditions. Because the results from the positive and negative experiments are nearly reversed, so we only present the results from the positive sensitivity experiment (SEN) in this paper.

For the second experiment, CAM5 is forced by historical global SST and sea ice with interannual variability from 1979 to 2013. The SST is a blended version of the HadISST dataset (Hurrell et al. 2008). This experiment is referred to as AMIP_EXP. The other forcing variables such as greenhouse gases and volcanic aerosols are set to climatological mean to avoid their effects on global precipitation.

3 Relationship between SWC rainfall and North Atlantic SST during boreal spring

In this section, we first analyze the climatological mean MAM rainfall in SWC. Figure 1c shows that MAM rainfall mainly occurs in the eastern part of SWC (exceeding 70 mm mon^{-1}). In addition, no significant rainfall is observed in the west-central part of SWC. On the other hand, compared to the north-central regions, the standard deviation of rainfall is more pronounced in the eastern and southern parts of SWC (Fig. 1d).

To identify the leading mode of the MAM rainfall anomalies in SWC, we perform EOF analysis on the rainfall anomalies using the station data. The EOF analysis is carried out on the covariance matrix. The first leading mode (EOF1) accounts for 31.73% of the total variance. According to the rule of North et al. (1982), EOF1 is well separated from the remaining modes. Therefore, EOF1 is considered statistically distinguishable and significant. Figure 2a shows the spatial pattern of EOF1. It is clear that EOF1 is characterized by a monopole structure. The loadings of EOF1 decrease from the southern to the northern part of SWC. When the principal component of EOF1 (PC1) (Fig. 2c, red line) is in the positive phase, SWC is dominated by positive rainfall anomalies,

Table 1 Positive and negative MAM NAI years based on ±0.5 standard deviation

Positive years	Negative years
1980, 1981, 1982, 1990, 1997, 1998, 1999, 2000, 2002, 2004, 2007, 2008	1979, 1983, 1986, 1987, 1993, 1994, 1996, 2010, 2012, 2013, 2015, 2016

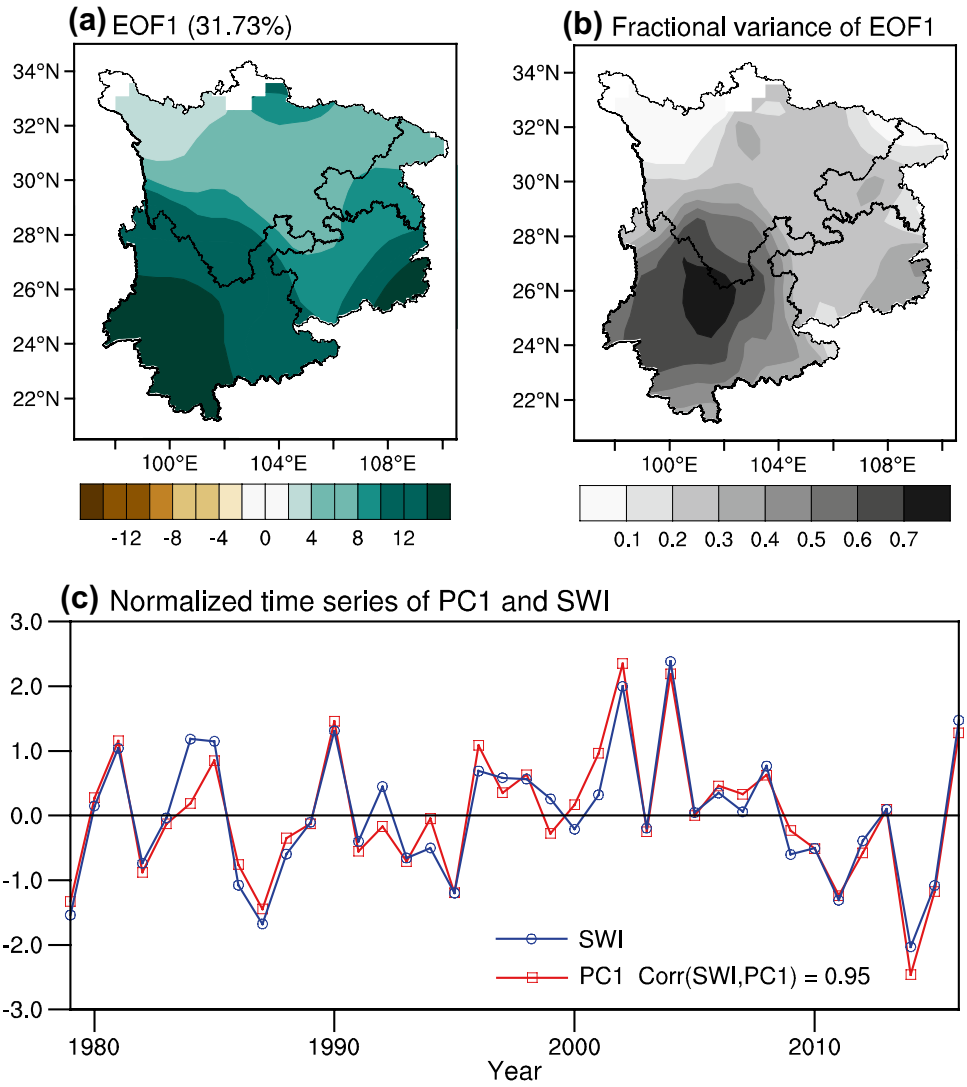

Fig. 2 **a** The leading EOF mode of MAM rainfall anomalies (mm mon^{-1}) in SWC during the period 1979–2016. **b** Fractional variances of MAM rainfall anomalies accounted for by the leading EOF mode. **c** Normalized time series of the first principal component (PC1) (*colored bars*) and SWI (*solid black line*)

implying more anomalous rainfall, and vice versa. Although EOF1 accounts for 31.73% of the total variance, the fractional variances explained by EOF1 vary with location. Figure 2b shows the spatial distribution of the fractional variances for EOF1. It is found that EOF1 accounts for more than 70% of the total variance in the southern part of SWC but explains less than 20% of the total variance in the northern part (north of about 29°N).

In the following, the SWC rainfall index (SWI) during boreal spring is defined as the station-averaged rainfall based on the 26 stations (black filled dots) shown in Fig. 1b. The normalized time series of SWI is shown in Fig. 2c (blue line). It is noted that PC1 and SWI show remarkable covariability. The correlation coefficient between PC1 and SWI is 0.95 (exceeding the 99% confidence level based on the Student's *t* test), indicating that SWI can well represent MAM rainfall variability in most of SWC.

To reveal the relationship between SWC MAM rainfall and the simultaneous North Atlantic SST, Fig. 3b presents the MAM SST pattern regressed onto the MAM SWI. It is evident that significantly positive regression coefficients exceeding the 90% confidence level based on the Student's *t* test mainly cover the mid-high latitude of the North Atlantic, indicating an in-phase relationship between SWC rainfall and North Atlantic SST during boreal spring. This feature suggests that positive rainfall anomalies appears in SWC during boreal spring when positive MAM SST anomalies appear in the mid-high latitude of North Atlantic.

Based on the above analyses, North Atlantic index (NAI) is defined as the area-averaged SST anomalies in the mid-high latitude of the North Atlantic (45°–65°N, 30°W–10°E), where SST anomalies exceed the 90% confidence level based on the Student's *t* test in Fig. 3b. Figure 3a presents the normalized time series of NAI (red line). It is clear that NAI and SWI show remarkable covariability. The correlation coefficient between NAI and SWI is 0.41 (exceeding the 99% confidence level based on the Student's *t* test) (Table 2), further indicating that a

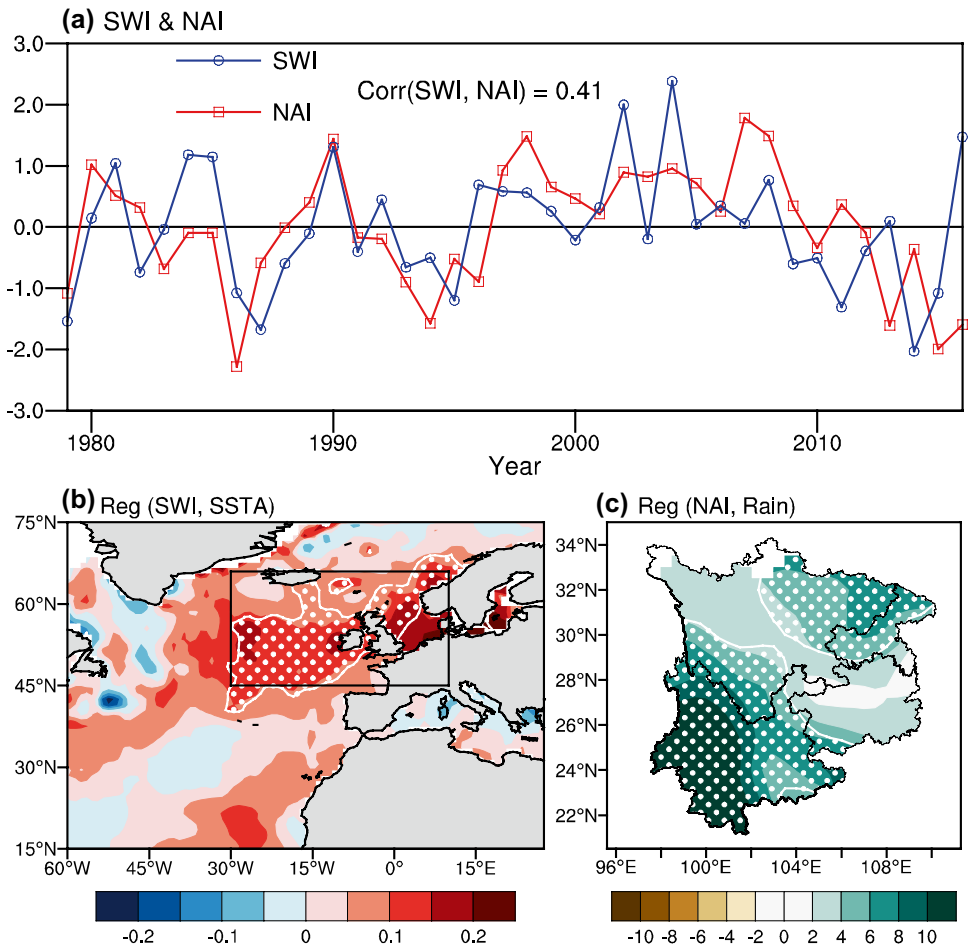

Fig. 3 **a** The normalized time series of SWI (*blue line*) and North Atlantic SST index (NAI) (*red line*) during boreal spring. Their correlation coefficient is also shown. **b** Regression pattern of MAM SSTA (°C) with respect to SWI. **c** Regression pattern of MAM rainfall (mm mon^{-1}) in SWC onto NAI. The *white contours filled with white dots* in **b** and **c** denote significance exceeding the 90% confidence level based on the Student's *t* test. The *black rectangle* (45°–65°N, 30°W–10°E) over North Atlantic in **b** is used to define the NAI

Table 2 Correlation coefficients between NAI, SWI, NRTCI and EAWRI

	NAI	SWI	NRTCI	EAWRI
NAI	1	–	–	–
SWI	**0.42**	1	–	–
NRCTI	**0.61**	**0.53**	1	–
EAWRI	0.31	0.13	**0.45**	1

The bold values exceed the 99% confidence level based on the Student's *t* test

significant in-phase relationship between SST in the mid-high latitude of North Atlantic and SWC rainfall during boreal spring. On the other hand, it should be mentioned that both SWI and NAI show interannual and interdecadal variations to some extent. This may require further research into their relationship on these two time scales, but this is beyond the scope of the present study.

To further investigate the relationship between SWC rainfall and North Atlantic SST during boreal spring, Fig. 3c presents MAM rainfall anomalies in SWC obtained by regression upon the MAM NAI. Positive rainfall anomalies dominates in most parts of SWC, with maximum rainfall anomalies in the south part of SWC, suggesting that MAM rainfall increases in SWC associated with the warm SST anomalies in the mid-high latitude of the North Atlantic during boreal spring. The regression pattern suggests that MAM North Atlantic SST may exerts a pronounced impact on the simultaneous rainfall in SWC, i.e., when SST in the mid-high latitude of the North Atlantic shows anomalous warming in MAM, the simultaneous SWC rainfall tends to increase.

To further demonstrate the coupled relationship between MAM North Atlantic SST and the simultaneous SWC rainfall, CCA analysis is applied to MAM North Atlantic SST (10.5°–79.5°N, 80.5°W–19.5°E) and SWC rainfall in MAM. The first leading mode (Fig. 4) accounts for 43% of the total covariance. The correlation coefficient between the time series of SST and rainfall (Fig. 4c) is 0.54 (exceeding the 99% confidence level based on the Student's *t* test). The North Atlantic SST signal exhibits a tri-pole pattern and is characterized by the feature of the significantly positive SST anomalies in the mid-high latitude of North Atlantic. The MAM rainfall field in SWC has significantly positive signal in most parts of SWC except for western

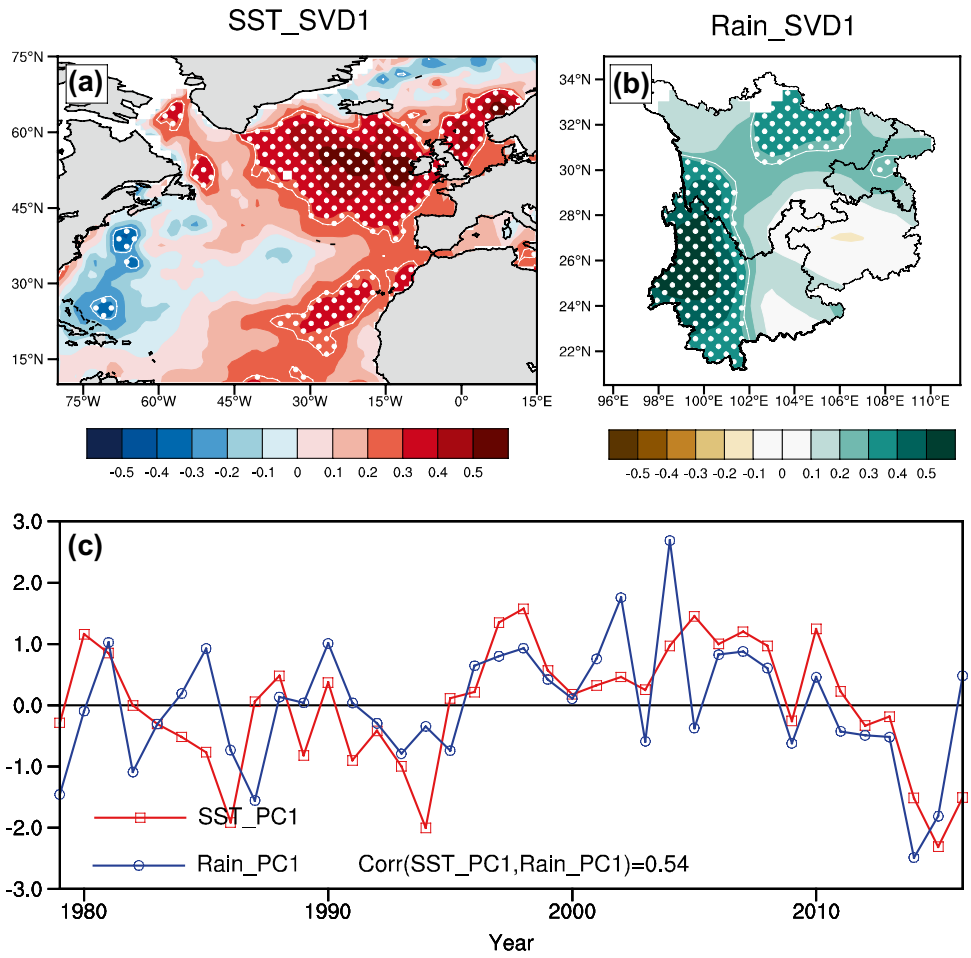

Fig. 4 The first leading CCA homogeneous modes of **a** the MAM SST in North Atlantic and **b** the simultaneous rainfall in SWC and **c** the normalized time series of the first leading CCA mode. The *white contours filled with white dots* represents significance exceeding the 90% confidence level based on the Student's *t* test

and northern part of SWC. When the North Atlantic SST is anomalous warming, positive rainfall anomalies appears in SWC. This further supports the above results that the boreal spring North Atlantic SST may influence the simultaneous SWC rainfall.

4 Possible physical explanation

From the analysis in Sect. 3, it can be inferred that boreal spring North Atlantic SST may influence the simultaneous SWC rainfall. It is well known that rainfall variability is often related to variability of atmospheric circulation and subsequent moisture transport. Therefore, we now explore the possible physical mechanisms that may be responsible for this relationship in this section based on analyses of atmospheric variables (wind, geopotential height, and so on) at different levels.

Figure 5 shows MAM wind anomalies at different vertical levels (200, 500 and 700 hPa) obtained by regression upon MAM NAI. It can be seen that the regression pattern of 200 hPa wind anomalies exhibits a significant teleconnection pattern extending from the mid-high latitude of North Atlantic to SWC (Fig. 5a). This teleconnection pattern is characterized by two anomalous anticyclones over the mid-high latitude of North Atlantic and the western Tibetan Plateau, and two anomalous cyclones over the western Russia and SWC, respectively. These anomalous atmospheric circulations form an arching wave train extending from North Atlantic to SWC. We refer to this teleconnection pattern as the North Atlantic–western Russia–western Tibetan Plateau–SWC (NRTC) teleconnection pattern. At 500 hPa (Fig. 5b), the regression pattern of wind anomalies still exhibits the NRTC teleconnection pattern, which is similar to that shown at 200 hPa. At 700 hPa (Fig. 5c), the anomalous cyclone covers most of southern Tibetan Plateau. To the southeast of the anomalous cyclone is an anomalous westerly or southwesterly wind, which is favorable for moisture transport from BOB to SWC, and thus resulting in more anomalous rainfall in SWC.

We also calculate the regression of MAM geopotential height anomalies at different levels (200, 500 and 700 hPa) upon MAM NAI (figure not shown). The regression patterns of geopotential height anomalies at different levels also exhibit the NRTC teleconnection pattern, which shows two positive geopotential height anomalies centers over the

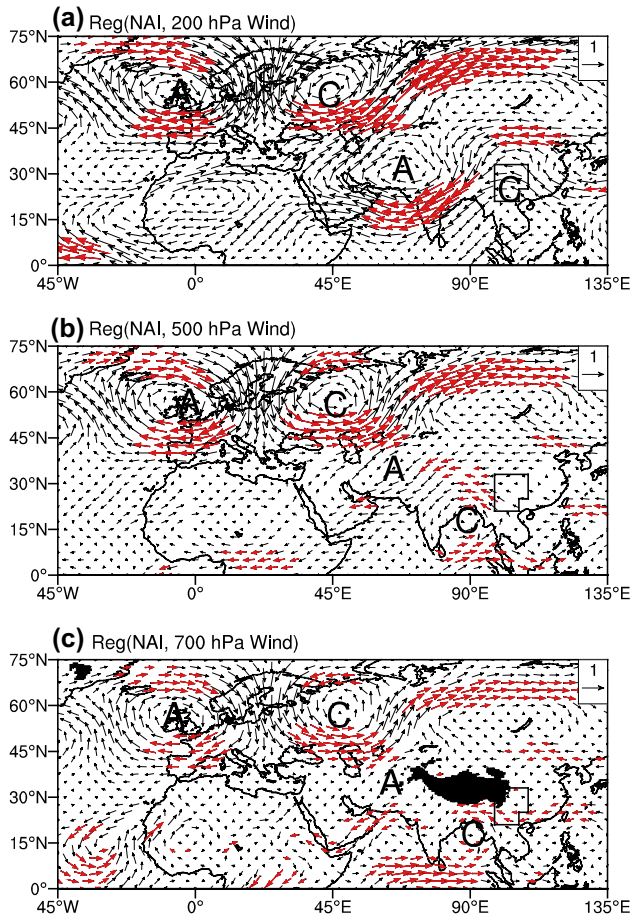

Fig. 5 Regression patterns of MAM wind (m s^{-1}) at **a** 200 hPa, **b** 500 hPa and **c** 700 hPa onto NAI. The *red vectors* indicate zonal winds exceeding the 90% confidence level based on the Student's *t* test. The *black shading areas* in **c** indicate the topography exceeding 3000 m

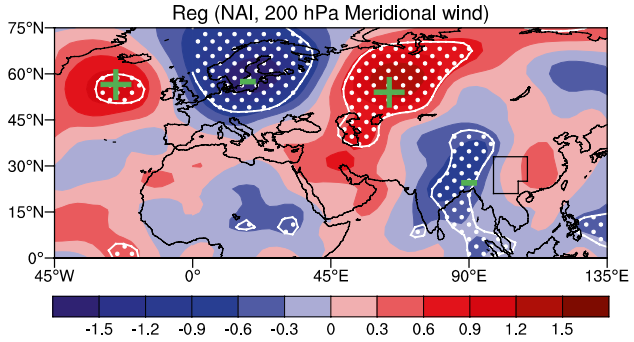

Fig. 6 Regression patterns of MAM meridional wind (m s^{-1}) at 200 hPa onto NAI. The *white contours filled with white dots* represents significance exceeding the 90% confidence level based on the Student's *t* test

mid-high latitude of North Atlantic and western Tibetan Plateau, and two negative centers over the eastern Russia and SWC. It should be mentioned that the NRTC teleconnection pattern is more significant at upper level than low level.

In addition, the NRTC teleconnection pattern is clearer in the 200 hPa meridional wind. Figure 6 presents the MAM meridional wind anomalies at 200 hPa obtained by regression upon MAM NAI. It is clear that the 200 hPa meridional wind anomalies exhibit a significantly arching wave train pattern extending from the North Atlantic to Tibetan Plateau. These results further demonstrate the existence of the NRTC teleconnection pattern from North Atlantic to SWC. Therefore, it can be concluded that MAM North Atlantic SST may influence the simultaneous SWC rainfall through the NRTC teleconnection pattern.

To further illustrate this NRTC teleconnection pattern, we define a NRTC teleconnection index (NRTCI) based on MAM averaged 200 hPa geopotential height anomalies using four points shown in Fig. 5a, which are marked by "A" (A: 10°W, 59°N), "C" (B: 44°E, 59°N), "A" (C: 68°E, 32°N) and "C" (D: 103°E, 25°N) extending from North Atlantic to SWC:

$$NRTCI = H200_A + H200_C - H200_B - H200_D \quad (3)$$

The normalized time series of NRTCI is presented in Fig. 7a (red line). It is clear that NRTCI shows interannual and interdecadal variabilities to some extent. Figure 7b presents MAM geopotential height anomalies at 200 hPa obtained by regression upon MAM NRTCI. This regression pattern exhibits a wave train structure extending from the mid-high latitude of North Atlantic to SWC, consisting of two positive centers over the mid-high latitude of North Atlantic and western Tibetan Plateau, and two negative centers over the eastern Russia and SWC. This indicates that NRTCI can accurately represent the structure of the teleconnection wave train extending from North Atlantic to SWC. Besides, the correlation coefficients between NRTCI, NAI and SWI are calculated to further reveal their relationship. The correlation coefficients of NRTCI with NAI and SWI are 0.61 and 0.53 (extending the 99% confidence level) (Table 2) during boreal spring; this proves that the impact of MAM North Atlantic SST on MAM rainfall in SWC may be conveyed through the NRTC teleconnection wave train.

On the other hand, it should be mentioned that the East Atlantic/West Russia (EA/WR) teleconnection pattern is an important atmospheric teleconnection pattern extending from western Europe to northern Asia (Barnston and Livezey 1987), bridging North Atlantic SST and East Asian climate during boreal winter (Wang et al. 2011; Lim and Kim 2013; Kim et al. 2013; Lim 2015). However, the role of EA/WR teleconnection pattern in connecting the boreal spring North Atlantic SST with the simultaneous SWC rainfall is unclear. Therefore, it is

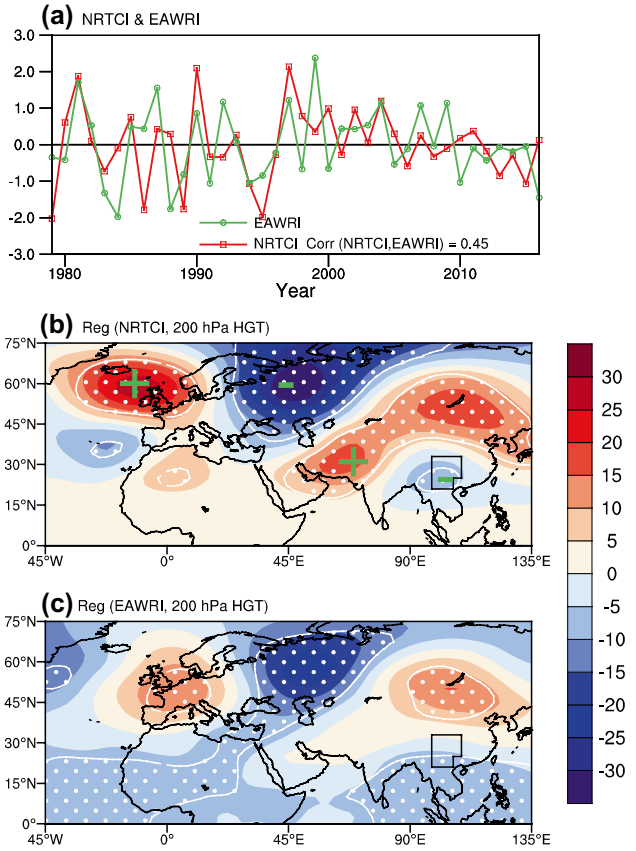

Fig. 7 **a** The normalized time series of NRTCI and EAWRI during boreal spring. **b** Regression patterns of MAM geopotential height at 200 hPa onto NRTCI. **c** Regression patterns of MAM geopotential height at 200 hPa onto EAWRI. The *white contours filled with white dots* represents significance exceeding the 90% confidence level based on the Student's *t* test

necessary to investigate this role. Figure 7c presents the EA/WR pattern, which is the regression pattern of MAM 200 hPa geopotential height anomalies upon MAM EA/WR index (EAWRI). The EA/WR pattern bears resemblance to the NRTC pattern to some extent. Indeed, the correlation coefficient between NRTCI and EAWRI is 0.45 (exceeding the 99% confidence level) (Table 2), indicating the significant relationship between these two patterns. However, unlike NRTC pattern, the correlation coefficients of EAWRI with NAI and SWI are 0.31 and 0.13 (Table 2), respectively, suggesting that the connection of EAWRI with NAI and SWI is very weak. Therefore, we can infer that the impact of North Atlantic SST on southwestern China rainfall during boreal spring may be not conveyed by EA/WR teleconnection pattern. However, further investigation is needed. Based on the correlation analysis results, it is indicated that MAM North Atlantic SST may influence the simultaneous rainfall in southwestern China through NRTC pattern rather than EA/WR pattern.

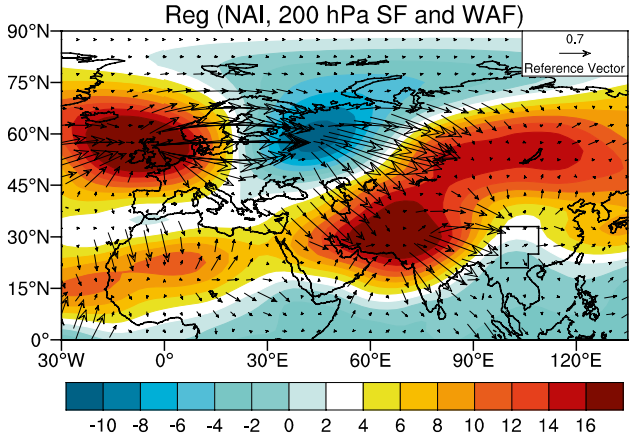

Fig. 8 Regression patterns of MAM streamfunction (*shading*, 10^6 m^2 s^{-1}) and wave activity flux (*vector*, m^2 s^{-2}) at 200 hPa onto NAI

The centers of NRTC teleconnection pattern are associated with the planetary Rossby wave energy propagation. The wave energy can propagate along the westerlies eastward to East Asia because the mid-latitude westerlies act as a Rossby waveguide (Hoskins and Ambrizzi 1993). Therefore, to elucidate the propagation of wave energy associated with NRTC teleconnection pattern, the wave activity flux (WAF) is examined. Figure 8 shows regression patterns of MAM streamfunction (SF) and WAF anomalies at 200 hPa onto MAM NAI. The regression pattern of SF and WAF shows a clear wave train accompanying energy transport extending from North Atlantic through western Russia and western Tibetan Plateau to SWC. This pattern suggests that the NRTC teleconnection pattern reflects Rossby waves responding to forcing of the mid-high latitude of North Atlantic SST. Therefore, it is further suggested that the North Atlantic SST during boreal spring can influence the simultaneous SWC rainfall through the NRTC teleconnection pattern.

We further calculate the MAM vertical velocity (omega) anomalies at 500 hPa obtained by regression upon MAM NAI (figure not shown). The regression pattern shows significantly anomalous ascending motion over SWC, indicating enhanced convective activity, and providing an important dynamic condition, which is favorable for positive rainfall anomalies in SWC. It should be mentioned that the MAM vertical velocity anomalies at 500 hPa is consistent with and explains the regression pattern of MAM rainfall in SWC (Fig. 3c).

We also calculate the MAM vertically integrated moisture flux (from surface to 300 hPa) anomalies obtained by regression upon MAM NAI (figure not shown). The vector of the moisture flux shows significant moisture transport from the BOB to SWC. Besides, SWC is associated with significantly anomalous moisture convergence,

corresponding to positive rainfall anomalies in SWC. Note that both the moisture flux and its divergence are also consistent with the regression pattern of MAM rainfall anomalies in SWC (Fig. 3c).

5 Numerical experiments

The observational analysis indicates that the NRTC teleconnection pattern could be responsible for the connection between the MAM North Atlantic SST and the simultaneous rainfall in SWC. In this section, numerical experiments are used to investigate whether or not the North Atlantic SST during boreal spring can influence the simultaneous SWC rainfall by the NRTC teleconnection pattern.

Considering that the NRTC teleconnection pattern is clearer in the upper atmosphere, the response of upper atmosphere to the North Atlantic SST is presented. Figure 9 presents the composite differences of the MAM geopotential height at 200 hPa based on the CLIM_EXP (SEN minus CTL). It is clear that the response of MAM geopotential height in the upper atmosphere to the simultaneous North Atlantic SST is generally similar to the results of observed analysis (Fig. 7b), showing a clear NRTC teleconnection pattern. The positive North Atlantic SST anomalies can excite a wave train extending from North Atlantic to SWC, with two positive centers over the mid-high latitudes of North Atlantic and the western Tibetan Plateau, and two negative centers over the western Russia and SWC, respectively. Corresponding to the distribution of geopotential height, the response of MAM 200 hPa wind to the simultaneous North Atlantic SST is also nearly consistent with the observational results (Fig. 10a), with two anomalous anticyclones over the mid-high latitudes of North Atlantic and the western Tibetan Plateau, and two anomalous cyclones over the western Russia and SWC, respectively. In addition, it should be mentioned that the response of MAM streamfunction and wave activity flux at 200 hPa to the simultaneous North Atlantic SST also displays a wave train extending from North Atlantic through western Russia and western Tibetan Plateau to SWC (Fig. 10b), which is similar to the result shown in Fig. 8. The above results provide a physical mechanism for the MAM North Atlantic SST influencing the simultaneous SWC rainfall through the NRTC teleconnection pattern: the positive MAM North Atlantic SST can excite a NRTC teleconnection pattern by which the North Atlantic SST results in positive rainfall anomalies in SWC (Fig. 11).

In fact, there are some differences between Figs. 3c and 11. Figure 3c shows the NAI-related MAM rainfall anomalies in SWC in observation, and Fig. 11 shows simulated MAM rainfall anomalies in SWC in the model. There are some differences between Figs. 3c and 11. The model results (Fig. 11) fail to simulate the positive rainfall anomalies over the northeastern part of SWC. Compared with Fig. 3c, the simulated maximum of positive rainfall anomalies in the west part of SWC in Fig. 11 shifts northward. Although the differences of spatial pattern of rainfall anomalies are seen, the correlation coefficient between the area-averaged rainfall anomalies in the SWC and the North Atlantic SST anomalies in the AMIP_EXP experiment is as high as 0.53 (extending the 99% confidence level) (Fig. 12), indicating that the impacts of North Atlantic SST on the SWC rainfall can be simulated and confirmed by the model. Therefore, the simulated spatial pattern of rainfall is acceptable. Such

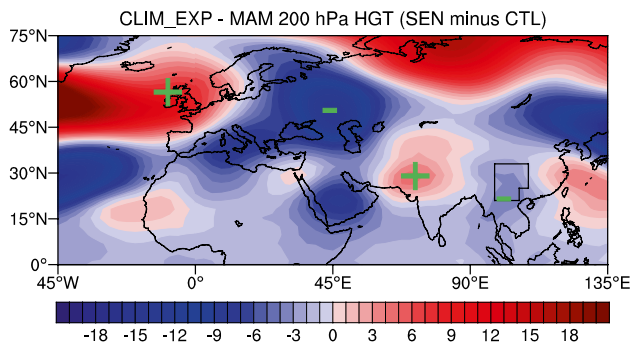

Fig. 9 Composite difference of MAM geopotential height (gpm) at **a** 200 hPa and **b** 500 hPa between SEN and CTL response to the North Atlantic SST forcing in the CAM5 model

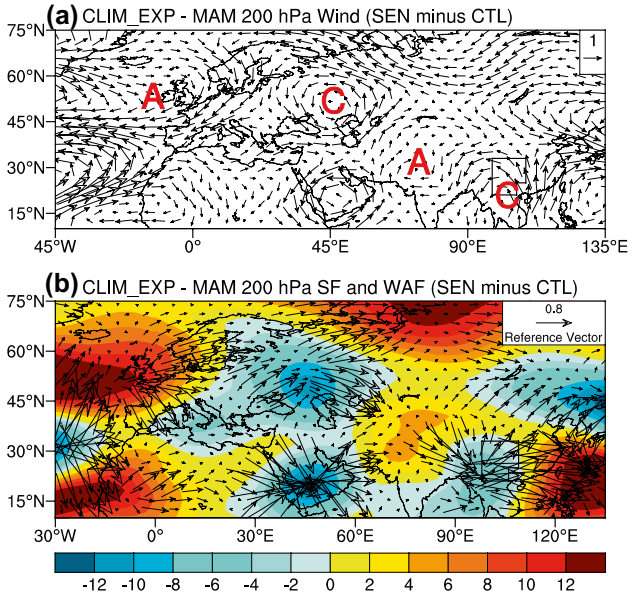

Fig. 10 Composite difference of MAM **a** wind and **b** streamfunction (*shading*) and wave activity flux (*vector*) at 200 hPa between SEN and CTL response to the North Atlantic SST forcing in the CAM5 model

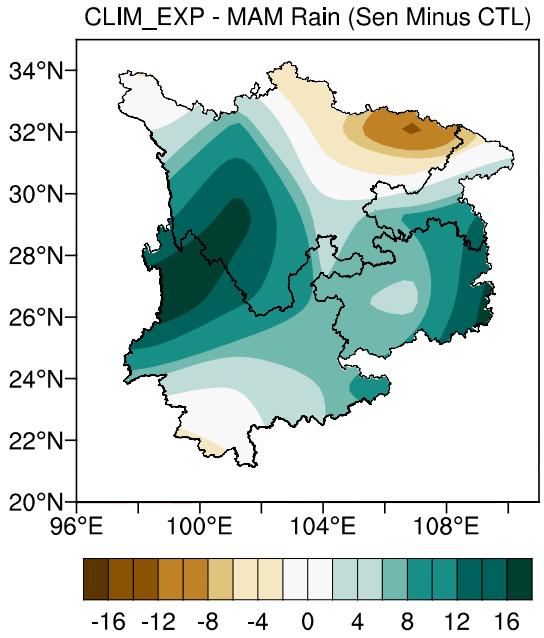

Fig. 11 Composite difference of MAM rain (mm mon^{-1}) in SWC between SEN and CTL response to the North Atlantic SST forcing in the CAM5 model

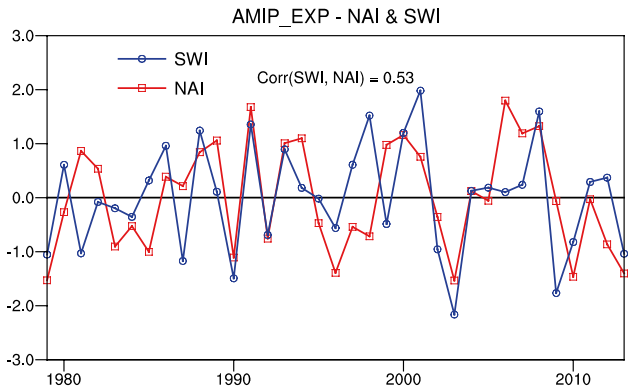

Fig. 12 The normalized time series of SWI (*blue line*) and North Atlantic SST index (NAI) (*red line*) during boreal spring in EXP_AMIP. Their correlation coefficient is also shown

differences of the spatial pattern of rainfall anomalies between simulations and observations may be related to the simulation ability of CAM5 model. Besides, although the amplitudes of the simulated rainfall are more than the observed, the simulated climatology displays the clear pattern with east–west gradient of rainfall (figure not shown), which is similar to the observed in Fig. 1c. However, compared with Fig. 1c, the simulated rainfall over the northeastern part of SWC is remarkably overestimated, indicating that the performances of CAM5 model in the northeastern part of SWC with complex topography (Fig. 1a) are not as good as in other region and need to be improved. These description and explanation are added in the revision.

The above two numerical experiments confirm that the MAM North Atlantic SST is an important factor that can influence the boreal spring rainfall in SWC. Within this process, the NRTC teleconnection pattern plays an important role.

6 Summary and discussion

In this study, we focused on the relationship between the boreal spring North Atlantic SST and the simultaneous SWC rainfall from 1979 to 2013 based on observational rainfall from Chinese weather stations and reanalysis data. This study demonstrates that as an important oceanic signal, the North Atlantic SST not only has an influence on climate variability over Northeast China (Wu et al. 2011) and East China (Gu et al. 2009; Wang et al. 2011) but also can affects the climate variability over SWC through the teleconnection atmospheric circulation pattern.

The results identify that there is a significant positive correlation between the boreal spring North Atlantic SST and the simultaneous SWC rainfall. When the boreal spring North Atlantic SST is anomalous warming, most of SWC is dominated by increased rainfall in MAM. The relationship between the boreal spring North Atlantic SST and the simultaneous SWC rainfall is further examined. Regression analyses show that negative 500 hPa geopotential height anomalies tend to appear over southern Asia when the boreal spring North Atlantic SST is anomalous warming. At 700 hPa, an anomalous cyclone can be observed over the BOB. This anomalous cyclone can favor moisture transport from the BOB to SWC, and significant anomalous moisture convergence appears in SWC. In addition, SWC is associated with significant anomalous ascending motion, providing an important dynamic condition for rainfall. The above results are favorable for positive rainfall anomalies in SWC during boreal spring.

Possible mechanisms for how North Atlantic SST influences SWC rainfall in SWC during boreal spring are further investigated. To resolve this issue, we investigated the distribution of atmospheric circulation over Eurasia associated with North Atlantic SST during boreal spring. Evidence presented here suggests that the boreal spring North Atlantic can induce a significant teleconnection wave train extending from the mid-high latitude of North Atlantic to SWC. When the boreal spring North Atlantic SST is anomalous warming, a North Atlantic–western Russia–western Tibetan Plateau–SWC (NRTC) teleconnection wave train appears from upper level to low level. At low level, two anomalous anticyclones are found over the mid-high latitude of North Atlantic and the western Tibetan Plateau,

and two anomalous cyclones are observed over the western Russia and BOB, respectively. The anomalous cyclone over BOB favors moisture transport to SWC, and thus results in positive rainfall anomalies in SWC during boreal spring.

Further investigations suggest that the NRTC teleconnection pattern is associated with the planetary Rossby wave energy propagation. When the boreal spring North Atlantic SST is anomalous warming, a clear Rossby wave train accompanying energy transport extends from North Atlantic through western Russia and western Tibetan Plateau to SWC. Therefore, the forcing of the mid-high latitude North Atlantic SST during boreal spring can be transmitted to SWC by the NRTC teleconnection pattern, and thus result in the anomalous cyclone over BOB, which can affect the rainfall over SWC.

On the basis of the above results, the CAM5 model is used to demonstrate the influence of North Atlantic SST on SWC rainfall during boreal spring. The simulated results are strongly in phase with the observation. The numerical experiments further confirm that the MAM North Atlantic SST is an important factor that can influence the boreal spring rainfall in SWC. Within this process, the NRTC teleconnection pattern plays a bridging role.

Finally, these results reveal that the North Atlantic SST may be an important predictor for SWC climate during the boreal spring based on observational and reanalysis data. However, how the North Atlantic SST anomalies influence the rainfall variability over SWC is a very complicated question. The North Atlantic SST anomalies may influence the rainfall variability over SWC by many other ways. For example, many previous studies have demonstrated that the influence of North Atlantic can be conveyed to northern Asia through the teleconnection pattern (Wang et al. 2011; Lim 2015), and then the influence can be further transported from northern to southern Asia through the thermal contrast (Dai et al. 2013). Besides, some scientific issues still remain. For instance, this study focuses only on the boreal spring. Therefore, the seasonality of the relationship between North Atlantic SST and SWC rainfall is the major focus of the following study. At last, whether the link between the North Atlantic SST and SWC rainfall is influenced by other climatic systems (e.g., SST in Indian Ocean and Pacific, El Niño, and so on) also needs to be studied.

Acknowledgements Gang Li acknowledges support from Prof. Jianping Li. The authors are very grateful for the valuable comments from three anonymous reviewers, which helped greatly in improving this paper. This work is jointly supported by the Strategic Priority Research Program of the Chinese Academy of Sciences (Grant No. XDA11010403), the CAS/SAFEA International Partnership Program for Creative Research Teams, the National Natural Science Foundation of China (NSFC) (Grants 41422601, 41521005, 41475070, 41490642 and 41575097), the National Basic Research program of China (Grant 2013CB956203), and the Science Foundation of Yunnan Province (Grant 2016FA041).

References

Barnston AG, Livezey RE (1987) Classification, seasonality and persistence of low-frequency atmospheric circulation pattern. Mon Weather Rev 115:1083–1126

Bretherton CS, Smith C, Wallace JM (1992) An intercomparison of methods for finding coupled patterns in climate data. J Clim 5:541–560

Cao J, Yao P, Wang L, Liu K (2014) Summer rainfall variability in low-latitude highlands of China and subtropical Indian Ocean dipole. J Clim 27:880–892. doi:10.1175/JCLI-D-13-00121.1

Cheng JG, Yan HM, Yan HS (2009) Analysis on characteristic and cause of severe climate disaster in Yunnan. China Meteorology Press, Beijing, p 250 **(Chinese)**

Dai A, Li HM, Sun Y, Hong LC, Ho L, Chou C, Zhou TJ (2013) The relative roles of upper and lower tropospheric thermal contrasts and tropical influences in driving Asian summer monsoons. J Geophys Res Atmos 118:7024–7045

Enfield DB, Mestas-Nunez AM, Trimble PJ (2001) The Atlantic multidecadal oscillation and its relation to rainfall and river flows in the continental US. Geophys Res Lett 28:2077–2080

Feng L, Li T, Yu WD (2014) Cause of severe droughts in Southwest China during 1951–2010. Clim Dyn 43:2033–2042. doi:10.1007/s00382-013-2026-z

Gu W, Li CY, Wang X, Zhou W, Li WJ (2009) Linkage between mei-yu precipitation and North Atlantic SST on the decadal timescale. Adv Atmos Sci 26(1):101–108

Hoskins BJ, Ambrizzi T (1993) Rossby wave propagation on a realistic longitudinally varying flow. J Atmos Sci 38:1179–1196

Huang RH, Liu Y, Wang L, Wang L (2012) Analyses of the causes of severe drought occurring in Southwest China from the fall of 2009 to the spring of 2010. Chin J Atmos Sci 36(3):443–457 **(Chinese)**

Hurrell JW, Hack JJ, Shea D, Caron JM, Rosinski J (2008) A new sea surface temperature and sea ice boundary dataset for the community atmosphere model. J Clim 21:5145–5153

Jiang XW, Li YQ (2011) Spatio-temporal variability of winter temperature and precipitation in Southwest China. J Geogr Sci 21(2):250–262. doi:10.1007/s11442-011-0842-9

Jiang XW, Yang S, Li J, Li Y, Hu H, Lian Y (2013) Variability of the Indian Ocean SST and its possible impact on summer western North Pacific anticyclone in the NCEP Climate Forecast System. Clim Dyn 41:2199–2212

Jiang XW, Li YQ, Yang S, Shu JC, He GB (2015) Interannual variation of mid-summer heavy rainfall in the eastern edge of the Tibetan Plateau. Clim Dyn 45:3091–3102. doi:10.1007/s00382-015-2526-0

Kalnay E et al (1996) The NCEP/NCAR 40-year reanalysis project. Bull Am Meteor Soc 77:437–471

Kim Y, Kim K-Y, Jhun J-G (2013) Seasonal evolution mechanism of the East Asian winter monsoon and its interannual variability. Clim Dyn 41:1213–1228. doi:10.1007/s00382-012-1491-0

Kim Y, Kim K-Y, Park S (2014) Seasonal scale variability of the East Asian winter monsoon and the development of a two-dimensional monsoon index. Clim Dyn 42:2159–2172. doi:10.1007/s00382-013-1724-x

Kushnir Y (1994) Interdecadal variations in North Atlantic sea surface temperature and associated atmospheric conditions. J Clim 7:141–157

Li YH, Xu HM, Bai YY, Li Q, He ZN (2010) Spatial–temporal characteristics of summer precipitation in the east of Southwest China. Plateau Meteor 29(2):523–530 **(in Chinese)**

Li YH, Lu CH, Xu HM, Cheng BY, Wang Y (2011) Contemporaneous relationships between summer atmospheric heat source

over the Tibetan Plateau and drought/flood in eastern Southwest China. Chin J Atmos Sci 35(3):422–434 **(Chinese)**

Li XZ, Zhou W, Li CY, Song J (2013) Comparison of the annual cycles of moisture supply over Southwest and Southeast China. J Clim 26:10139–10158. doi:10.1175/JCLI-D-13-00057.1

Lim Y-K (2015) The East Atlantic/West Russia (EA/WR) teleconnection in the North Atlantic: climate impact and relation to Rossby wave propagation. Clim Dyn 44:3211–3222. doi:10.1007/s00382-014-2381-4

Lim YK, Kim HD (2013) Impact of the dominant large-scale teleconnections on winter temperature variability over East Asia. J Geophys Res 118:7835–7848. doi:10.1002/jgrd.50462

Liu Y, Zhao EX, Peng GF, Yang SQ (2007) Severe drought in the early summer of 2005 in Yunnan and middle-high latitudes circulation. Arid Meteor 25: 32–37

Liu T, Li JP, Zheng F (2015) Influence of the boreal autumn Southern annular mode on winter precipitation over land in the Northern Hemisphere. J Clim 28:8825–8839. doi:10.1175/JCLI-D-14-00704.1

Ma ZF, Peng J, Gao WL, Tian H (2006) Climate variations of Southwest China during the last century. Plateau Meteor 25(4): 633–642 **(in Chinese)**

Mao LX, Qian S, Hou YY, Li CS (2007) Study on the meteorologically-driven ecological monitoring and assessment of high temperature and drought of Sichuan-Chongqing area in summer 2006. Meteorol Mon 33: 86–88

Plumb RA (1985) On the three-dimensional propagation of stationary waves. J Atmos Sci 42:217–229

Qin J, Ju JH, Xie ME (1997) Weather and climate in low latitudes plateau. China Meteorology Press, Beijing, p 210 **(Chinese)**

Rayner NA et al (2003) Global analyses of sea surface temperature, sea ice, and night marine air temperature since the late nineteenth century. J Geophys Res 108(D4):4407. doi:10.1029/2002JD002670

Song J, Li CY, Zhou W (2014) High and low latitude types of the downstream influences of the North Atlantic Oscillation. Clim Dyn 42:1097–1111. doi:10.1007/s00382-013-1844-3

Tao Y, Cao J, Hu J, Dai Z (2013) A cusp catastrophe model of mid-long-term landslide evolution over low latitude highlands of China. Geomorphology 187:80–85. doi:10.1016/j.geomorph.2012.12.036

Wang X, Wang D, Zhou W (2009) Decadal variability of twentieth century El Niño and La Niña occurrence from observations and IPCC AR4 coupled models. Geophys Res Lett 36:L11701. doi:10.1029/2009GL037929

Wang X, Wang CZ, Zhou W, Wang DX, Song J (2011) Teleconnected influence of North Atlantic sea surface temperature on the El Niño onset. Clim Dyn 37:663–676. doi:10.1007/s00382-010-0833-z

Wang X, Zhou W, Li CY, Wang DX (2012) Effects of the East Asian summer monsoon on tropical cyclones genesis over the South China Sea on an interdecadal timescales. Adv Atmos Sci 29:249–262

Wang WW, Zhou W, Wang X, Fong SK, Leong KC (2013a) Summer high temperature extremes in Southeast China associated with the East Asian jet stream and circumglobal teleconnection. J Geophys Res Atmos 118:8306–8319

Wang X, Wang CZ, Zhou W, Liu L, Wang DX (2013b) Remote influence of North Atlantic SST on the equatorial westerly wind anomalies in the Western Pacific for initiating an El Niño event: an atmospheric general circulation model study. Atmos Sci Lett 14:107–111

Wang X, Zhou W, Wang DX, Wang CZ (2013c) The impacts of the summer Asian Jet Stream biases on surface air temperature in mid-eastern China in IPCC AR4 Models. Int J Climatol 33:265–276

Wu ZW, Zhang P (2015) Interdecadal variability of the mega-ENSO-NAO synchronization in winter. Clim Dyn 45:1117–1128. doi:10.1007/s00382-014-2361-8

Wu ZW, Wang B, Li J, Jin FF (2009) An empirical seasonal prediction model of the East Asian summer monsoon using ENSO and NAO. J Geophys Res 114:D18120. doi:10.1029/2009JD011733

Wu RG, Yang S, Liu S, Sun L, Lian Y, Gao ZT (2011) Northeast China summer temperature and North Atlantic SST. J Geophys Res 116:D16116. doi:10.1029/2011JD015779

Wu ZW, Li JP, Jiang ZH, He JH, Zhu XY (2012) Possible effects of the North Atlantic Oscillation on the strengthening relationship between the East Asian summer monsoon and ENSO. Int J Climatol 32:794–800

Xu HL, Li JP, Feng J, Mao JY (2012) The asymmetric relationship between the winter NAO and the precipitation in Southwest China. Act Meteorol Sin 70(6):1276–1291 **(in Chinese)**

Yan HM, Lu YB, Cheng JG, Duan H, Yang SY (2005) The impact of preceding atmospheric circulation and SST variation on flood season rainfall in Yunnan. J Trop Meteor 11:121–130

Yan HM, Li QQ, Sun CH, Yuan Y, Li D (2013) Criterion for determining the onset and end of the rainy season in Southwest China. Chin J Atmos Sci 37(5):1111–1128 **(Chinese)**

Yang J, Gong DY, Wang WS, Hu M, Mao R (2012) Extreme drought event of 2009/2010 over southwestern China. Meteorol Atmos Phys 115:173–184. doi:10.1007/s00703-011-0172-6

Yu J-Y, Kao P-K, Peak H, Hsu H-H, Huang C-W, Lu M-M, An S-I (2015) Linking emergence of the central Pacific El Niño to the Atlantic multidecadal oscillation. J Clim 28:651–662. doi:10.1175/JCLI-D-14-00347.1

Zhang WL, Zhang JY, Fan GZ (2014) Dominant modes of dry- and wet-season precipitation in southwestern China. Chin J Atmos Sci 38(3):590–602 **(Chinese)**

Zheng F, Li JP, Li YJ, Zhao S, Deng DF (2016) Influence of the Summer NAO on the Spring-NAO-based predictability of the East Asian summer monsoon. J Clim 55:1459–1476. doi:10.1175/JAMC-D-15-0199.1

Zou XK, Gao H (2007) Analysis of severe drought and heat wave over the Sichuan Basin in the summer of 2006. Adv Clim Chang Res 3:149–153 **(in Chinese)**